Detection of Artificial Satellites in Images Acquired in Track Rate Mode.

Martin P. Lévesque

Defence R&D Canada- Valcartier, 2459 Boul. Pie-XI North, Québec, QC, G3J 1X5 Canada,
martin.levesque@drdc-rddc.gc.ca

ABSTRACT

For surveillance of space needs, satellites must be re-observed periodically to measure their position and update their orbital parameters. This represents an incredible volume of data for which an automatic processing capability is desired. Previous developments [1,2,3] produced automatic detection algorithms for images acquired in Step Stare mode (SSM) with sidereal tracking. However, it was proven that the track rate mode (TRM) [6] is more sensitive. Hence, the algorithmic framework was redesigned and applied to this mode.

When an imaging sensor tracks a satellite (or a satellite cluster), the stars appear as streaks while the satellites are point-like objects. A series of algorithms was developed for the detection of satellites and star streaks. The centroids of the star streaks are first detected. They are necessary for the astrometric calibration of the image. Thereafter, the satellites are detected using two sets of logical conditions; they are detected with the maximum of sensitivity against the dark sky background, and with the contrast criteria if they are overlapping star streaks. This algorithm framework automatically extracts all required information from the image and adapts the processing parameters and strategy consequently, so no a priori knowledge is require for their execution, which is a requirement for automatic processing capacity.

1. Introduction

The maintenance of the Space Surveillance Network (SSN) catalogue of space resident objects (RSO) requires an incredible amount of fresh observations. Thousands of objects need to be observed almost every month. This is done by several observatories (optical and radar) which must acquired hundreds of observations every nights. This represents a huge amount of image data that must be analyzed and reduced to observation update reports.

The goal of the recent development of the Canadian sensor array [4] is the creation of autonomous observatories which could do the entire job automatically. Ultimately, the optical sensors (ground or space based) should be operated by a single man, who checks the system status, error reports and consistency of observation reports. Presently, this goal is almost achieved. There is still system debugging and maintenance to do, but all the elements are in place and operational. When TLEs become too old, they pop up warnings in the SSN TLE database and new observations are requested. These requests are transmitted to the sensor operating center and the scheduler program generates the observation tasks. This program determines when a RSO will be observable by a specific observatory, and it generates command sequence that will control all components of the observatory necessary to perform the TLE update. These command sequences are uploaded into the observatory controlling computer. Once the observatory has performed its task, the images are downloaded and processed with the automatic detection algorithms presented in this paper. The detections are reported to SSN and the TLE database is updated. At the moment, all these processes can be done completely automatically.

The RSO observation can be done in several different modes. Automatic image processing algorithms [1,2,3] were developed for the step stare mode (SSM), or sidereal tracking. But this acquisition mode is not used anymore because the track rate mode (TRM) is more sensitive and is now almost the only used acquisition mode. Therefore, the processing scheme had to be rearranged to process images taken in TRM rather than SSM mode. These TRM images are characterized by streak-like stars and point-like satellite. In this new image processing framework, the image background is first removed as in SSM processing, but the star streaks are filtered before trying detecting the satellite. Once the stars are adequately filtered, they are removed from the background-free image and the remaining point objects become apparent and easily detectable. This paper presents an overview of this processing.

2. Image Model and processing frame work

The image acquired by the CCD camera contains several separable components. It is composed of a background component 'B' (the sum of the ADC (analog to digital converter) bias, stray light, zodiacal light and light pollutions), a series of star streaks 'S', a series of pin point objects (the tracked satellites) 'O' and noise 'n'. The model of the original image 'I^0' is:

$$I^0 = B + S + O + n \qquad (1)$$

The goal of the processing method is the separation of the significant satellite signals 'O' from the other components. From these later, only the noise is purely stochastic and cannot be model otherwise than by its means and variance. The other components can be estimated with filtering techniques. The background can be accurately estimated '«B»' with an iterative estimation method [5], which, after subtraction, leaves only a background residue '$\mathcal{R}_B$' that is less than $\bullet_n/5$ [5]. Hence, the background-free image 'I^{-B}' is :

$$I^{-B} = \quad I^0 - \text{«B»} \quad = \quad S + O + \mathcal{R}_B + n. \qquad (2)$$

Once the star streak length 's_l' and orientation 's_θ' are known (with the Fourier-Radon method describe in section 4), an iterative matched filter '$\mathcal{M}$' [2] provides a very good estimate of the star streak image '«S»', which is free of noise.

$$[\text{«S»}, C] = \mathcal{M} (I^{-B}, s_l, s_\theta). \qquad (3)$$

This matched filter also provides an image 'C' of the streaks convolved by a calibrated line segment representing the ideal streak. These convolution peaks are also use later in the processing. For each streak, the maximum of the convolution peak provides the mean value of the streak intensity. Also, the position of this peak maximum provides the position of the streak centroid.

A streak-free image 'I^{-S}' is obtained by subtracting the filtered streak image «S» from the background-free image 'I^{-B}'. This resulting image 'I^{-S}' contains almost only the satellites along with processing residues ('$\mathcal{R}_S$' is the streak residues, i.e. '$\mathcal{R}_S = S - \text{«S»}$'):

$$I^{-S} = I^{-B} - \text{«S»} = O + \mathcal{R}_B + \mathcal{R}_S + n. \qquad (4)$$

The detection of the satellites is done by applying a combination of detection thresholds, '$\mathcal{T}$' , which depends on the noise level 'σ_n', width 'w_{psf}' of the optical PSF (point spread function) and on an estimate of the local streak residue «$\mathcal{R}_S$»:

$$\text{Detection criteria:} \quad \text{«O»} \quad > \quad (\mathcal{T}_S (\text{«}\mathcal{R}_S\text{»}) + \mathcal{T}_n (w_{psf}, \sigma_n)) \qquad (5)$$

Where, '«O»' is the best estimate of the satellite signal 'O'. With this model, without considering the PSF width, the closest value to 'O' is 'I^{-S}'. Otherwise, «O» can be the integration of 'I^{-S}' over an area corresponding to the PSF size. '$\mathcal{T}_n (w_{psf}, \sigma_n)$' is the threshold value for the noise and '$\mathcal{T}_S (\text{«}\mathcal{R}_S\text{»})$' the threshold value that is required to remove false alarms generated by streak residues. For the detection, the background residue '$\mathcal{R}_B$' is negligible and it is ignored in the present processing.

In this processing model, there are a certain number of functions that require detailed explanations to understand their principles and their performances. The iterative background estimation method and iterative matched filter were already published in Ref. [2]. The details of the calculation of the streak length and orientation (s_l, s_θ) are presented in ref. [6].

3. Satellite detection

The Fig. 1 shows the result of this processing model in a visually representative sequence. The processing does not occur exactly in the presented order, but presenting the results in this manner allows the illustration of the processing model (Equations. 1 to 5). The real processing begins by the star extraction presented in the section 4. Once the stars are adequately known, their knowledge is used to remove several false alarms. But for the interest of the reader, let's begin by the satellite detection.

In the example of Fig. 1, there is a bright satellite that overlaps a star streak. In the final image, the presence of the satellite is clearly visible. Detecting such a bright satellite is not an issue. The problem is the determination of

detection thresholds that allow a maximum of sensitivity and the detection of very faint satellites without increasing the false alarm rate. The difficulty relies in the presence of two kinds of background: 1) the empty space where only the image noise is perceptible and 2) the star streaks which may occult the satellite and are also a source of false alarms.
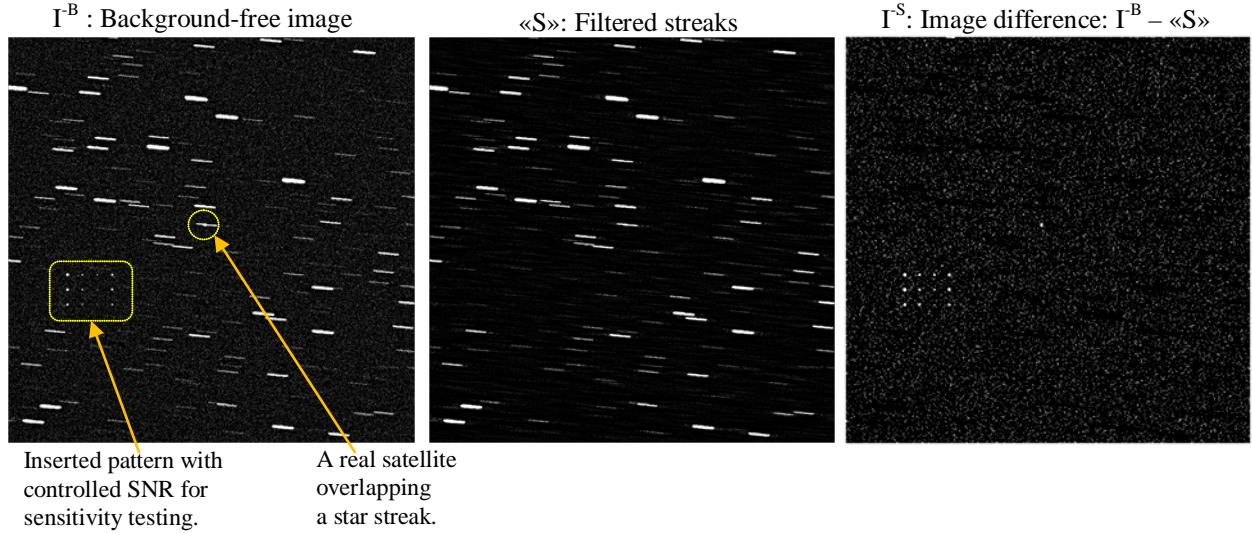
I^{-B} : Background-free image   «S»: Filtered streaks   I^{-S}: Image difference: I^{-B} – «S»

Inserted pattern with controlled SNR for sensitivity testing.

A real satellite overlapping a star streak.

Fig. 1. Separation of the image components

The setting of the noise threshold depends principally on the width of the PSF. The CCD detector noise is almost a perfect Gaussian noise. For faint signal, the Poison distribution of the photon noise is lower than the dark current and reading noise. For a Gaussian noise, it is well known that 3% of the statistic events are above the $2\sigma_n$ level, but it is less known that for 10^6 pixels, there may have one random event above 5 or $6 \sigma_n$ that generates a false alarm. This is without considering the CCD default like hot pixels. Therefore, for a very narrow optical PSF (less than one pixel), the safe threshold (for an almost zero false alarm rate) is set to $9\sigma_n$. A lower threshold value could be use for more sensitivity, but this is not desirable for an autonomous system which must not declare false alarms. This is for a detection based on a single pixel measurement. For larger PSF, the best signal estimation [3,6] is obtained when the signal is integrated (or summed) over an area equivalent to the PSF area. This averages the noise. Integration over a larger area only dilutes the signal with more background. Therefore, the best satellite estimation is:

$$\text{«O»} = \text{mean}_{NxN}(\text{I}^{-S}) \qquad (6)$$

where the subscript 'NxN' is the size of the local window ($N \approx w_{psf}$ in pixels) and the detection noise threshold is set to:

$$\mathcal{T}_n (w_{psf}, \sigma_n) = 9\sigma_n / N \qquad (7)$$

The streak residue '$\mathcal{R}_S$' that remains in the final image 'I^{-S}' is more complicate to handle. While the noise threshold is global to the image, the streak residue threshold is specific to the encountered streak. The filtered streaks, in the filtered image '«S»', are smooth functions while the original streaks 'S' are more textured, mostly due to the pixelisation of the signal. The residue intensity ($\mathcal{R}_S = S - \text{«S»}$) has variations higher than the noise level and is proportional to the intensity of the local streak. This is a strong source of false alarm. Several tests demonstrated that a high contrast value (satellite / star streak) must be used for the elimination these false alarms. The threshold value that does not generate false alarm was determined experimentally and set to:

$$\mathcal{T}_{S1} (\text{«}\mathcal{R}_S\text{»}) = 2 \text{«S»} \qquad (8)$$

i.e., the streak residue threshold is twice the value of the overlapping streak. There are two ways to define the threshold '$\mathcal{T}_S$' and both definitions are used sequentially. First, '$\mathcal{T}_{S1}$' (in Eq. 8) is the pixel-to-pixel comparison. It is quick to compute but generates several false alarms. Second, '$\mathcal{T}_{S2}$' is used for an object-to-object comparison. It is accurate but requires a more complex computing scheme. At the first pass, the pixel to pixel test is done by comparing the streak-free image 'I^{-S}' with the filtered streaks 'S'. This is a good test in the middle of the streak where the signal is strong. But, this generates several false alarms because the streak signal is faint in the streak periphery and where the signal pixelization is a great source of signal fluctuations. For the pixels that succeed this

first test, the second detection test with '$\mathcal{T}_{S2}$' is applied. For these pixels, the intensity is compared with the mean value of the nearest streak, i.e.:

$$\mathcal{T}_{S2}\ (\text{«}\mathcal{R}_{S}\text{»}) = 2 \text{ mean of nearest streak.} \qquad (9)$$

For this purpose, every streak is extracted and becomes an independent object. Its area is defined by a binary mask, which is defined in the next section. The nearest streak is the streak which has at least one pixel from its binary mask that overlap the target PSF area. If more than one streak is possibly in contact with the candidate pixel, the nearest one is chosen. This process eliminates the false alarms caused by the streak residues «$\mathcal{R}_{S}$».

Figure 2A shows an example of detected satellites (yellow circles in the left image) in an image acquired in the galactic plane. Figure 2B shows the centroids of the stars that were detected by the algorithms for the same image (described in next section). In this case, when these satellites were tracked, several images were acquired with a few seconds of interval and the same detections occurred in every frame, confirming that these detections are not false alarms.
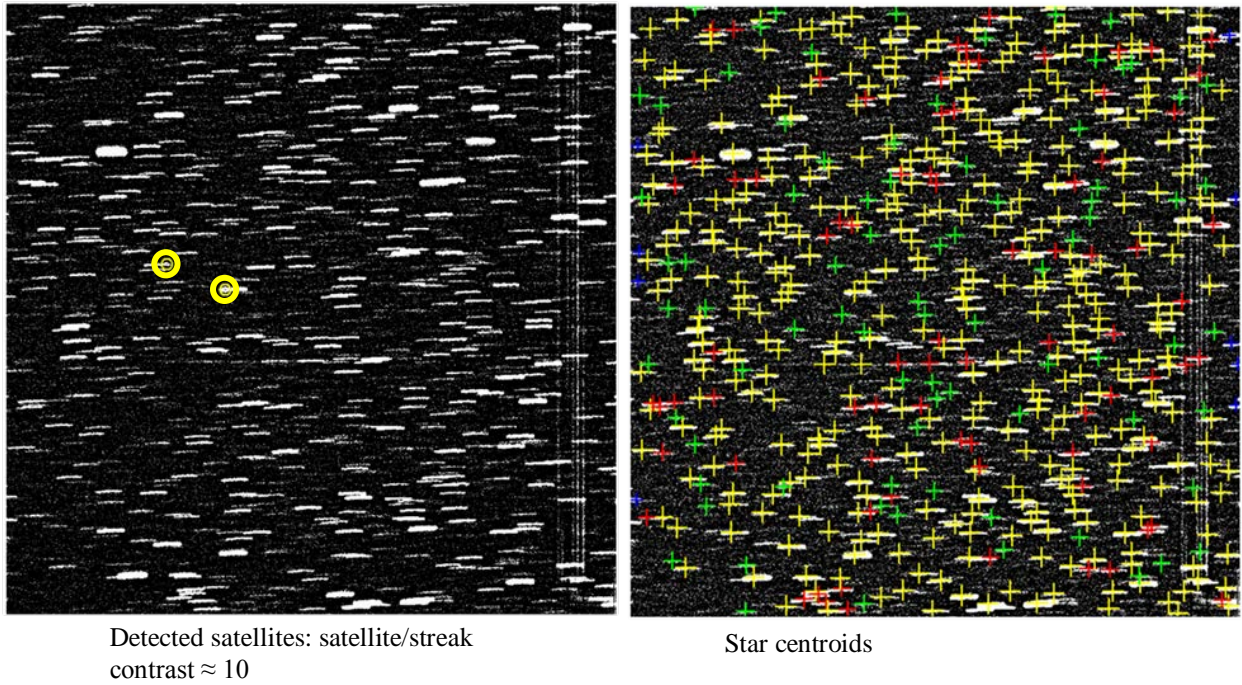

Detected satellites: satellite/streak
contrast ≈ 10

Star centroids

Fig. 2. A: Satellite detection (left) and B: star streak detection (right).

4. Star streak detection and measurement

The individual star streaks need to be extracted for two raisons. First, the satellite detection algorithms do not apply the same rules if the background is the empty space or an overlapping streak. Second, the knowledge of the star field is required to evaluate the astrometric position of the detected satellites. A simple threshold technique allows only the extraction of the brightest star streaks. Very often, there are not enough bright stars for the astrometry software [7] to converge toward an accurate solution. So a sensitive method is required to detect the faint stars. The images of Fig. 2 represent the other extreme case; there are too many stars and the confusion avoids the production of a unique result. This is why the galactic plane is an area that is usually avoid for satellite detection, but this image was a good image for processing testing.

The iterative matched filter [2] is the best method for the extraction of very faint streaks. However, it requires knowing the a priori streak length and orientation. Usually, this could be obtained from the metadata (pointing and tracking parameters) but there are so many streaks in the image that the algorithm can get this knowledge from the image content itself. Figure 3 shows how this can be done. When calculating the Fourier transform of an image containing several streaks, the modulus (ABSolute function) of the FFT contains the typical pattern shown in Fig. 3. A streak is like a 'Rectangle' function and the modulus of the FFT of a series of streaks produces the typical

$(\sin(x)/x)^2$ function. The sharpest profile and the strongest central peak are obtained when the directional integration is done with the appropriate orientation. This is indicated by the maximum value of the Radon transform of the modulus of the FFT. This angle is the orientation of the streaks 's_θ'. Finally, by measuring the position of the zeros of the $(\sin(x)/x)^2$ in the profile extracted at this angle, the frequency of the $\sin(x)$ function is solved and the length 's_l' of the 'rectangle' function is calculated. Detailed calculations are presented in ref. 6.

With (s_θ, s_l) known, the matched filter [2,6] calculates clean streaks '«S»' in presence of a severely-attenuated noise. In Eq. 3., the '$\mathcal{M}$' function also calculates the convolution peaks 'C' resulting of the streaks convolved by a 'rectangle' function, which is a representation of a perfect streak. The profiles of both raw streak and convolution peak are presented in Fig. 4. One may note that the maximum of the convolution peak correspond to the centroid of the star streak.

Image in TRM

ABS (FFT (image))

←FFT→

145 degrees

Extracted profile at 145 degrees

Radon (ABS (FFT (image)))

Central Radon profile

Maximum intensity of the extracted angle-dependent profiles
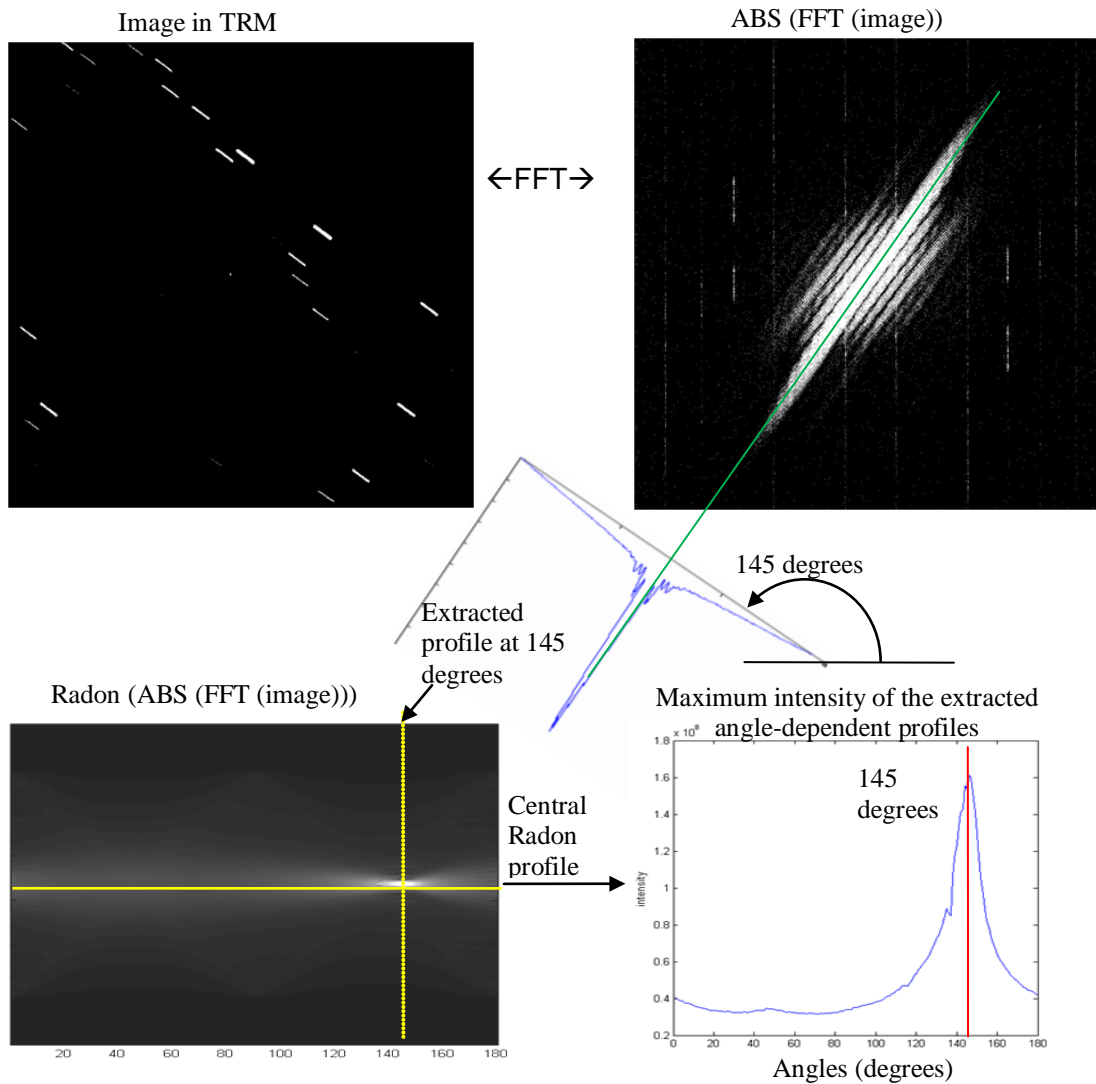
145 degrees

intensity

Angles (degrees)

Fig. 3. Determination of the streak orientation with the Radon transform of the modulus of the Fourier transform.

The position of a star centroid and its brightness are given by the position and amplitude of the maximum of its convolution peak (Fig. 4). But, before extracting these parameters, every streak areas must be delimited. This is done with a binary mask which is used to separate and label the individual streaks. Such a binary mask can be obtained by applying a threshold on the raw image or on the convolved image. Both methods have their advantages.

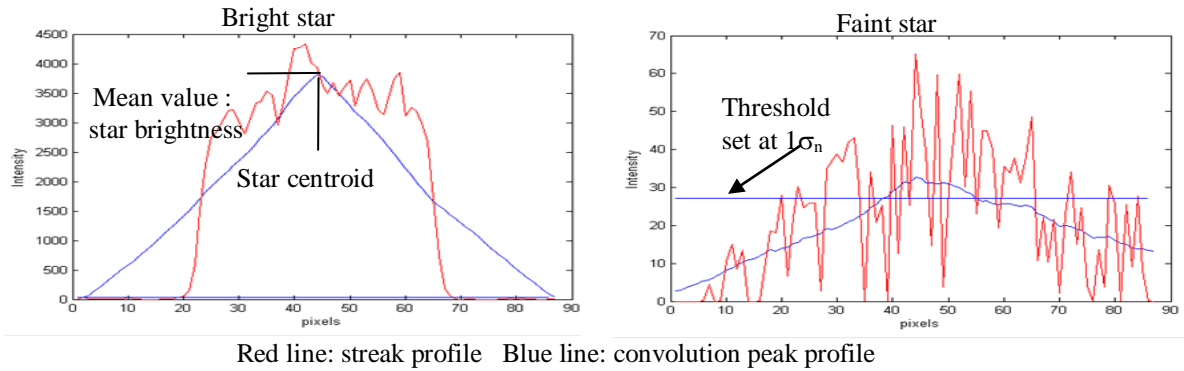Red line: streak profile   Blue line: convolution peak profile

Fig. 4. Profiles of raw streak and convolution peak for bright and very faint stars. Even for very faint stars, the convolution peak remains visible but not the raw profile.

The raw image generates sharp masks with the same size as the streaks. But they are noisy (Fig. 5) and they can extract only very bright streaks. They are the masks 'A' in Fig. 5. The convolved image can generate very smooth masks (masks 'B' in Fig. 5.), even for very faint stars. But their sizes are variable; they depend on the ratio between the streak brightness and the threshold value. Also, their larger sizes have the tendency of merging close streaks. The best solution consists in using both methods in cascade. The bright stars are extracted first with the sharp mask 'A'. They are measured (centroid position and brightness) and then erased from the image. Example of such centroid measurements are shown in Fig. 6, where the bright stars are identified with yellow crosshairs.
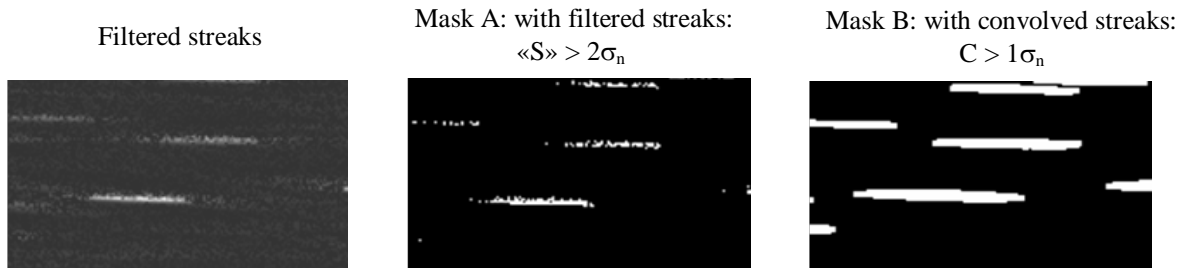

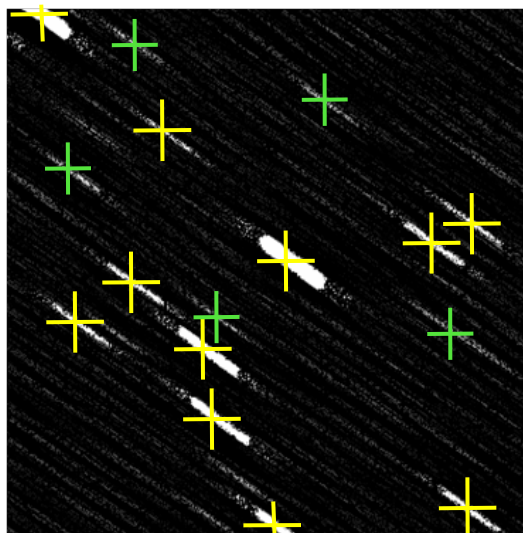Fig. 5. Creation of binary masks for the extraction of individual streaks.

Fig. 6. Bright stars detected with the sharp mask 'A' (yellow crosshairs) and faint stars detected with the sensitive mask 'B' (green crosshairs).

After the removal of the already detected bright stars, the remaining faint streaks are extracted with the second mask 'B'. Their centroids and amplitudes are also measured using their convolution peaks. The limit of sensitivity for the detection of faint streak is SNR=1 (example shown in Fig. 4). In Fig. 6, the streaks detected with the second pass are identified with green crosshairs. The same color code was used in Fig. 2. At the end of the processing, a list of detected stars is produces along with their positions and brightness. This is necessary for the calculation of the astrometric calibration of the scene. This is done with the 'PinPoint' commercial software [7]. This allows the conversion of image coordinates (line, sample) into sidereal coordinates (Ra, Dec).

Even though the streak length, s_l, has already been estimated with the FFT modulation (Fig. 3), a more accurate estimation can be obtained by measuring the streaks at half height. Figure 7 shows that the measurement of the streak width also provides a very good estimation of the image PSF. This PSF width is used for setting the detection conditions (size of integration area and averaged-noise dependent threshold) in Eqs. 6 and 7. Note that the PSF width can change in time (atmospheric turbulence, out of focus caused by thermal stress, etc.) and this method provides the real PSF measured from the image content.
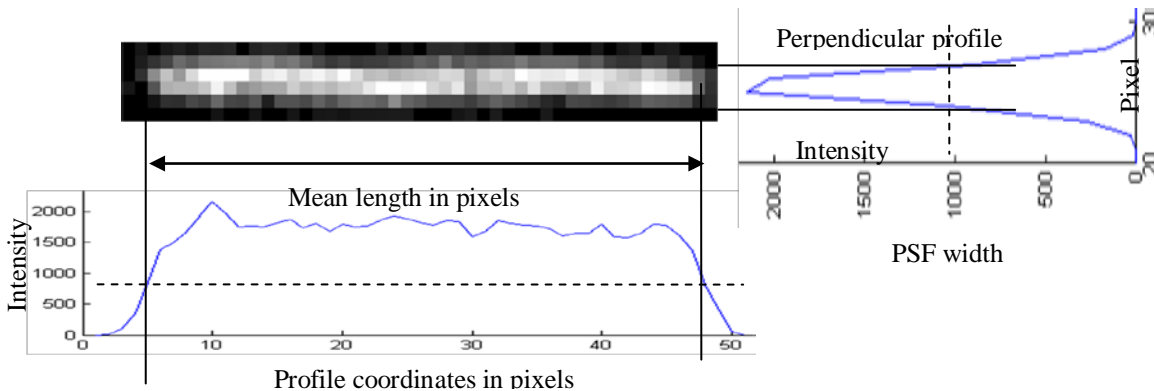

Fig. 7. Measurement of the streak length and width (PSF) at half height

The last problem that requires to be solved is the presence of merged star streaks. For the identification of the star field, a missing bright star in the detection report may confuse the astrometry software. Very often when stars are close enough, their extraction masks can be merged, producing a single object. When the object is much longer than expected, it is then obvious that it is the result of such a merging. In such a case, only the brightest of the merged streak is detected. Also, in this case, the position of the centroid is far away from the geometric center of the extraction mask and this is also used as an indication that this object is merged with another one. However, if the first detected streak is erased from the merged streaks, it then becomes possible to detect the second one. This is difficult to do in the filtered streak image (because of the textured signal) but this is easier with the smooth convolution peaks (Fig. 4).

Figure 8 illustrates the streak unmerging process. These two close streaks were extracted as a single object with a total length almost the double than the expected streak length. Also, when extracting the position of the maximum of the convolved streaks (streak convolved by the streak model, i.e., a line segment with the length 's_l' and orientation 's_θ'), the peak maximum is far from the geometric center of the mask. This clearly indicates where the first streak is and that this streak is not alone in this local extraction mask. This first convolution peak is erased by subtracting a modeled peak. It is obtained by convolving the streak model with itself. Note that this peak model is always the same for all detected stars. But, when a peak model is subtracted, it is always calibrated with the amplitude of the considered star. Hence, the first streak is erased and the second streak becomes clearly visible and detectable. This process can be repeated several times. It stops when the SNR of the remaining signal becomes too low or when the subtraction residue is too high, i.e. the model does not fit anymore with the remaining signal. Fig. 9 shows an example where three streaks were detected with this method. The first detection is indicated by the yellow crosshair. The following ones are indicated by red crosshairs. The details of this method are presented in Ref. [6].

This process performs very well for streaks with very high brightness difference. But it does not work if the streaks are too close, i.e., the separation is less than half a streak length and half a streak width. In such a case, the maximum of the overlapping convolution peaks does not indicate anymore the position of the brightest streak but a

position between the two inseparable merged streaks. For these cases, a more complex morphological analysis of the merged streaks is required. Even though this algorithm limit, it meets the actual need since it solves most of the encountered cases. It allows the calculation of the astrometric calibration of several images that, otherwise, would have been rejected.

A typical observation for the detection of a satellite is a 10 second exposure with a small telescope (Celestron 14) which has a FOV of 1 degree [4]. This type of automated system can acquire hundreds of images in a single night. Before the implementation of these algorithms, only the streak detection method using the sharp mask 'A' (defined if Fig. 5) was used. An important part of the observations was trashed (about 50%) because there were not enough bright stars to obtain a good astrometric solution for the calculation of the satellite position. With these new algorithms (two-pass detection method with sharp mask 'A' and sensitive mask 'B' and the unmerging method) the number of trashed observations has been reduced considerably to less than 10%.
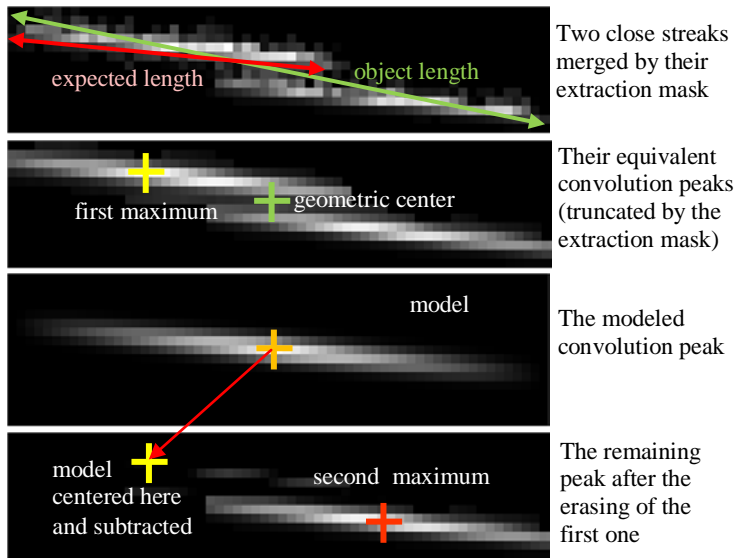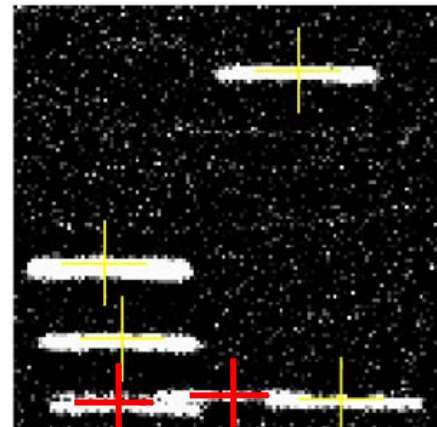

Fig. 8. Unmerging streaks

Example of unmerged streaks: the first one is marked by the yellow crosshair. Red crosshairs indicate the second and third ones.

Fig. 9. Example of unmerged streaks

5. Causes of processing failure

This algorithm framework is now integrated to the operating software of the Canadian observatories used for the surveillance of space. They have been tested for more than a year. There are still cases where the images are rejected for various raisons. Several tracking errors (during the acquisition) were responsible for processing failures. The kind of tracking errors that disturbed the processing are: telescope acceleration (the streak intensity is not constant), tracking maneuver (curved streak) or telescope vibration (spike in the middle of all streaks). In all these cases, the irregular streak shape makes the processing believes there are satellites overlapping all star streaks (all at the same place on the streaks), which obviously does not make sense. This false alarm/detected-streak correlation is easy to detect and reject. These cases are measurable and when they occur, it is, most of the time, effectively preferable to reject the acquisition.

The density of the star field is the other raison for the rejection of observations. The detection algorithms detect the satellites, but sometime it is not possible to calculate their positions. When not enough stars are detected, the astrometry software is not able of identifying the observed scene and is not able to link the image coordinates (of the detected objects) to real sidereal coordinates (Ra, Dec). The star-streak detection algorithms are designed to be the most sensitive as possible without generating false detections. Also a special attention was done for the unmerging of close stars. It is likely that the sensitivity cannot be increased with more processing. To minimize the rejection of images due to unsuccessful astrometry, the observation planning software (which is also an autonomous program) should include a constraint to assure that enough stars will be present in the FOV for each observation. This type of rejection occurred often with the previous (less sensitive) streak detectors, but, with these new algorithms, it is now

fairly rare. On the opposite, too many similar stars (of equal brightness) confuse the astrometry software and this occurs frequently. Many star of different brightness is not an issue because they can be ranked correctly. But in the example of Fig. 2, more than 500 stars were detected. Reducing the sensitivity (to detect fewer stars) does not solve the problem because there are too many stars with similar magnitude and angular separation. Once again, in these cases either, the observation planning was not optimized for the acquisition. Usually the galactic plane is an area where the system does not make acquisition because of this particular problem.

6. Conclusion

The algorithm framework for the automatic detection of satellites and star streaks is complete and performs very well. It was tested for more than one year and it was used to process thousand of images. It reduced considerably the image rejection (due to bad astrometric solution) and improves the system sensitivity by detecting fainter satellites. The sensitivity of the extraction and measurement of the stars and the satellites is close to the noise limit, but without declaring false alarms. For the cases where the satellite is overlapping a star streak, the detection is limited by the satellite/streak contrast. Otherwise, it is limited by the signal-to-noise ratio. The detection thresholds are dynamically adjusted with the PSF measured from the image content. Hence, if atmospheric conditions degrade the image quality (but the sky is still enough good for performing observations) the detection algorithms will remain as sensitive as possible.

The algorithms for the measurement of the centroids of the star streak are also very efficient. The streak orientation and length are measured from the image content, so the algorithms are completely autonomous and do not depend on external metadata. The star streaks are extracted by two different, but complementary, methods. The first one is less sensitive but produce sharp extraction masks. The second one produces larger masks but the sensitivity reaches the noise limit. A special attention was done for the extraction of several centroids when close stars generate merged streaks. The star positions are given by the maximum of the convolution peaks produced by the matched filter. The position of this convolution maximum is equivalent to a calculation of the center of mass of the extracted mask. All the signal (contained in the streak area) is used for the calculation, this produces the best estimate as possible and this process does not depends on an arbitrary pixel selection process (like the end-point measurement, a geometric center which depends on a threshold values, etc.).

It seems obvious that a track rate mode (TRM) acquisition is more sensitive than a sidereal step stare mode (SSM) acquisition. Here are the numbers to prove this. In SSM [6], it was established that a 130 pixels-long satellite streak (with a 3 pixel wide PSF) could be detected with a threshold set to $0.5\sigma_n$. Here, in TRM, the threshold of Eq. 7 is set to $3\sigma_n$ for a signal integrated over a 3x3 pixels area for the same PSF. Considering the total area of the target and the PSF intensity distribution, the brightness of object that can trig the detection threshold was calculated for both modes. It was calculated [6] that the object must be bright enough to generate $206\sigma_n$ pixel counts on the CCD in SSM (to generate a 130 pixel long streak above the $0.5\sigma_n$ threshold level), while only $45\sigma_n$ counts are necessary to trig detection in TRM (for a 3x3 average above the $3\sigma_n$ threshold level). Therefore, for the same PSF, the acquisition in TRM is 5 times more sensitive than an acquisition in SSM. This means that the detection system wins 2 visual magnitude of sensitivity when it operated in TRM. Also, for designing purpose, it should be underlined that an optical system with a PSF narrower than 1 pixel is also 5 times more sensitive than a 3 pixel wide PSF and this should drive the requirement. In other word, the integration of the signal over the PSF area increases the detection performance, but does totally compensated for optical blur.

Finally, the detection threshold values defined in this paper were adjusted for obtaining a maximum of sensitivity with 0% of false alarm. For a cueing mode, the threshold values could be lowered and the sensitivity increased, but these detection algorithms were designed for an autonomous system that is not allowed declaring false alarms.

7. References

1. Lévesque M.P.,: 'Automatic Reacquisition of Satellite Positions by Detecting Their Expected Streaks In Astronomical Images', 2009 AMOS Technical Conferences, 02 Sept. 2009, proceeding: 10 pages.
2. Lévesque M. P., Buteau S., Image Processing Technique for Automatic Detection of Satellite Streaks. DRDC Valcartier 2005 TR-386. Defence R&D Canada – Valcartier. http://cradpdf.drdc.gc.ca/PDFS/unc64/p527352.pdf , accessed Apr. 2011.
3. Lévesque M. P., Lelièvre M., Improving satellite-streak detection by the use of false alarm rejection algorithms. DRDC Valcartier TR 2006-587. Defence R&D Canada – Valcartier. http://pubs.drdc.gc.ca/PDFS/unc76/p530206.pdf , accessed Apr. 2011.
4. Wallace B., Rody J., Scott R., Pinkney F., Buteau S., Lévesque M. P., "A Canadian Array of Ground-Based Small Optical Sensors for Deep Space Monitoring", 2003 AMOS Technical Conference.
5. Lévesque M. P., Lelièvre M., Evaluation of the iterative methods for image background removal in astronomical images. DRDC Valcartier TN 2007-344. Defence R&D Canada – Valcartier. http://pubs.drdc.gc.ca/PDFS/unc69/p52905 4.pdf, accessed Apr. 2011.
6. Lévesque M. P., 'Image processing algorithms for the automatic detection of artificial satellites acquired in track rate mode (TRM)'. DRDC Valcartier TR 2010-052. Defence R&D Canada – Valcartier. Limited distribution.
7. http://pinpoint.dc3.com/, accessed Apr. 2011.